Quadratic Regularization Design for 3D Axial CT

Jang Hwan Cho and Jeffrey A. Fessler

Abstract—**While iterative reconstruction (IR) methods have potential advantages over conventional FBP reconstruction such as reduced patient dose and improved noise properties, their use of statistical weighting and space variant scanning geometries can lead to nonuniform and anisotropic spatial resolution. Due to the large number of voxels in the image volume, regularization design methods based on discrete Fourier transforms would require prohivitive computational cost. In this paper, we propose a quadratic regularization design method for 3D axial X-ray computed tomography (CT) that aims to improve resolution isotropy and uniformity. Simulations and a phantom experiment show that the proposed method leads to more uniform and isotropic spatial resolution in 3D axial CT with modest computational cost.**

I. INTRODUCTION

Improved noise and spatial resolution properties are one of the potential advantages of statistical image reconstruction methods over conventional filtered back-projection (FBP) reconstruction [1]. Regularized image reconstruction methods, such as penalized weighted least squares (PWLS) method or a penalized-likelihood (PL) method, provide noise control by integrating a roughness penalty into the cost function. Although statistical weighting and system models are responsible for improving image quality, their interaction with a conventional quadratic roughness penalty results in images as anisotropic and nonuniform spatial resolution. This holds even for idealized shift-invariant imaging systems [2], and becomes most severe near the end slices of 3D axial or helical CT.

Several previous regularization designs aim to match the local impulse response of the estimator to a target impulse response by matrix manipulations and discrete Fourer transforms [2], [3]. The matrix and FFT methods need too much computation when applied to an entire image volume. Expecially for 3D axial or helical CT. A fast analytical regularization design method for 2D fan-beam X-ray CT that uses continuous space analogs to simplify the regularization design problem was proposed in [4]. In [5], the authors addressed the problem for 3D axial CT, but for a simplified 3D system that was modeled as a stack of 2D fan-beam systems. In this paper, we propose a regularization design for 3D axial X-ray computed tomography (CT) accounting for cone angle. Simulations and a phantom experiment show that the proposed method leads to more uniform and isotropic spatial resolution in 3D axial CT with modest computational cost.

II. METHOD

A. Local Impulse Response

Consider a penalized weighted least squares (PWLS) objective function of the form

$$\Psi(\boldsymbol{x}) = \mathsf{L}(\boldsymbol{x}) + \mathsf{R}(\boldsymbol{x}), \quad \mathsf{L}(\boldsymbol{x}) = \frac{1}{2} \|\boldsymbol{y} - \boldsymbol{A}\boldsymbol{x}\|_{\boldsymbol{W}}^2, \quad (1)$$

where $\boldsymbol{y}$ is the measurement vector, $\boldsymbol{A}$ is the system matrix, $\boldsymbol{x} = (x_1, \cdots, x_N)$ is the discretized version of the object being imaged, and $\boldsymbol{W} = \mathrm{diag}\{w_i\}$ is a statistical weighting matrix. A conventional quadratic regularizer is expressed as

$$\mathsf{R}(\boldsymbol{x}) = \beta \sum_j \sum_{l=1}^{N_l} \kappa_{l(j)} \kappa_j r_j^l \frac{1}{2} \left((c_l * * * x)\, [n, m, z] \right)^2, \quad (2)$$

where index j is a lexicographical ordering of $[n, m, z]$, N_l is the number of neighbors (13 in 3D), c_l is a function performs finite differences between neighboring voxels (see (11) below), κ's are the user-defined weights [2] for controlling spatial resolution in the reconstructed image, and $\{r_j^l\}$ are the directional regularizer coefficients that we will design.

For a quadratic regularizer, the local impulse response (LIR) at the jth voxel for the PWLS estimator is given as:

$$l^j = [\boldsymbol{A}'\boldsymbol{W}\boldsymbol{A} + \boldsymbol{R}]^{-1} \boldsymbol{A}'\boldsymbol{W}\boldsymbol{A}\boldsymbol{\delta}_j, \quad (3)$$

where $\boldsymbol{R}$ is the Hessian of the regularizer $\mathsf{R}(\boldsymbol{x})$ and $\boldsymbol{\delta}_j$ denotes an impulse function at jth voxel [2]. Our purpose is to design $\boldsymbol{R}$ such that our local impulse response l^j matches a target l^o that has more isotropic spatial resolution, at every pixel j. We simplify this process by turning to the frequency domain.

Assuming $\boldsymbol{A}'\boldsymbol{W}\boldsymbol{A}\boldsymbol{\delta}_j$ and $\boldsymbol{R}\boldsymbol{\delta}_j$ are approximately locally circulant [6], we can approximate (3) as follows:

$$L^j = \frac{F\left(\boldsymbol{A}'\boldsymbol{W}\boldsymbol{A}\boldsymbol{\delta}_j\right)}{F\left(\boldsymbol{A}'\boldsymbol{W}\boldsymbol{A}\boldsymbol{\delta}_j\right) + \beta F\left(\boldsymbol{R}\boldsymbol{\delta}_j\right)}, \quad (4)$$

where $F(\cdot)$ denotes the 3-D DFT.

Instead of directly using the discrete Fourier transform, we use the continuous-space analog of $H_j \triangleq F\left(\boldsymbol{A}'\boldsymbol{W}\boldsymbol{A}\boldsymbol{\delta}_j\right)$ in spherical coordinates $\boldsymbol{\nu} \triangleq (\rho, \Phi, \Theta)$. We use a closed-form approximation for H_j that was suggested in [7]:

$$
\begin{aligned}
H_j(\boldsymbol{\nu}) &\approx K J(\boldsymbol{\nu}) \frac{\tilde{w}_j(\Phi)}{\rho \cos(\Theta)} \quad (5) \\
K &= \Pi \Delta_x^3 \Delta_z D_{sd}^2 / D_{so}^2 \\
J(\boldsymbol{\nu}) &= \mathrm{sinc}(\Delta_x \rho \cos(\Theta) \cos\Phi)^2 \\
&\quad \times \mathrm{sinc}(\Delta_y \rho \cos(\Theta) \sin\Phi)^2 \mathrm{sinc}(\Delta_z \rho \sin(\Theta))^2 \\
\tilde{w}_j(\Phi) &= \sum_{\beta \in B_j(\Phi)} \frac{\bar{w}_{\beta,j}}{d_{\beta,j} \sqrt{1 - (\zeta^j \cos(\theta^j))^2 \cos^2(\phi^j - \Phi)}},
\end{aligned}
$$

where $D_{so} \cdot (\zeta^j, \phi^j, \theta^j)$ denotes the location of the jth voxel in spherical coordinates, K is a constant depending on voxel

sizes and scanner geometry, $J(\boldsymbol{\nu})$ is a factor depending only on spatial frequencies, $\bar{w}_{\beta,j} \triangleq w_\beta(\bar{s}_j^*)$ where $\bar{s}_j^*$ is the positon on the detector that maximizes the footprint of voxel j at source angle β, $d_{\beta,j}$ is the distance from the source to the xy-projection of voxel j, and $B_j(\Phi)$ is the set of the values of β for which the ray passing through voxel j is perpendicular to the frequency vector $\boldsymbol{\nu}$ where the ray and frequency vector are both projected onto the xy-plane [7]. Substituting (6) into (4) yields the following expression for the continuous space analog of L^j:

$$L^j \approx \frac{KJ(\boldsymbol{\nu})\tilde{w}_j(\Phi)/(\rho\cos(\Theta))}{KJ(\boldsymbol{\nu})\tilde{w}_j(\Phi)/(\rho\cos(\Theta)) + \beta R_j(\boldsymbol{\nu})}, \tag{6}$$

where $R_j(\boldsymbol{\nu})$ is the local frequency response for the regularizer near pixel j (see (15) below).

B. Target Impulse Response

The local frequency response associated with penalized unweighted reconstruction is isotropic at the isocenter for a full scan, so we use it as our target response. At isocenter, (6) for uniform weights ($w_i = 1$) is given as

$$\begin{aligned} H_o(\boldsymbol{\nu}) &\approx KJ(\boldsymbol{\nu})\frac{\tilde{u}_o(\Phi)}{\rho\cos(\Theta)}, & (7)\\ \tilde{u}_o(\Phi) &= |B_j(\Phi)|. \end{aligned}$$

Now the target local frequency response is

$$L^o \approx \frac{KJ(\boldsymbol{\nu})\tilde{u}_o(\Phi)/(\rho\cos(\Theta))}{KJ(\boldsymbol{\nu})\tilde{u}_o(\Phi)/(\rho\cos(\Theta)) + \beta R_o(\boldsymbol{\nu})}, \tag{8}$$

where L^o is the continuous-space analog of L^o.

Our purpose is to match the local impulse response at jth voxel to the target impulse resonse, i.e., we want

$$\begin{aligned} L^j &\approx \frac{KJ(\boldsymbol{\nu})\tilde{w}_j(\Phi)/(\rho\cos(\Theta))}{KJ(\boldsymbol{\nu})\tilde{w}_j(\Phi)/(\rho\cos(\Theta)) + \beta R_j(\boldsymbol{\nu})} & (9)\\ &\approx \frac{KJ(\boldsymbol{\nu})\tilde{u}_o(\Phi)/(\rho\cos(\Theta))}{KJ(\boldsymbol{\nu})\tilde{u}_o(\Phi)/(\rho\cos(\Theta)) + \beta R_o(\boldsymbol{\nu})} \approx L^0. \end{aligned}$$

Cross multiplying and simplifying yields the goal

$$\tilde{u}_o(\Phi)R_j(\boldsymbol{\nu}) \approx \tilde{w}_j(\Phi)R_o(\boldsymbol{\nu}). \tag{10}$$

C. Regularization Structure

We first define a first-order differencing function that penalizes lth neighbor as

$$c_l = \frac{1}{\sqrt{n_l^2 + m_l^2 + z_l^2}}(\delta(n, m, z) - \delta(n - n_l, m - m_l, z - z_l)), \tag{11}$$

where n_l, m_l, z_l denote the offset of the neighbor. Taking the Fourier transform of (11) yields the following expression for the local frequency response $|C_l(\omega_1, \omega_2, \omega_3)|^2$

$$\begin{aligned} &= \frac{1}{n_l^2 + m_l^2 + z_l^2}\left|1 - e^{-i(\omega_1 n_l + \omega_2 m_l + \omega_3 z_l)}\right|^2\\ &= \frac{1}{n_l^2 + m_l^2 + z_l^2}\left(2 - 2\cos(\omega_1 n_l + \omega_2 m_l + \omega_3 z_l)\right). \tag{12} \end{aligned}$$

Using the approximation $2 - 2\cos(x) \approx x^2$ [4] (12) simplifies

$$|C_l(\omega_1, \omega_2, \omega_3)|^2 \approx \frac{1}{n_l^2 + m_l^2 + z_l^2}(\omega_1 n_l + \omega_2 m_l + \omega_3 z_l)^2. \tag{13}$$

We convert (13) to spherical frequency coordinates. The relationship between frequency and sampling yields $\omega_1 = 2\pi\Delta_x\rho\cos(\Phi)\cos(\Theta)$, $\omega_2 = 2\pi\Delta_y\rho\sin(\Phi)\cos(\Theta)$, and $\omega_3 = 2\pi\Delta_z\rho\sin(\Theta)$. Substituting these into (13) yields the following expression for $|C_l(\omega_1, \omega_2, \omega_3)|^2$

$$\begin{aligned} \approx \frac{1}{n_l^2 + m_l^2 + z_l^2}(2\pi\rho)^2 (n_l\Delta_x\cos(\Phi)\cos(\Theta)\\ + m_l\Delta_y\sin(\Phi)\cos(\Theta) + z_l\Delta_z\sin(\Theta))^2 \tag{14} \end{aligned}$$

The local frequency response of the regularizer (2) is now

$$R_j(\rho, \Phi, \Theta) = (2\pi\rho)^2\kappa_j^2\sum_{l=1}^{N_l} r_j^l \left(e(\Phi, \Theta) \cdot [e(\Phi_l, \Theta_l) \otimes \Delta]\right)^2, \tag{15}$$

where $e(\Phi, \Theta) \triangleq (\cos(\Phi)\cos(\Theta), \sin(\Phi)\cos(\Theta), \sin(\Theta))$, $\Delta \triangleq (\Delta_x, \Delta_y, \Delta_z)$, $\otimes$ is element-wise multiplication, and we assumed that $\kappa_j \approx \kappa_l$ for l within the neighborhood of j.

For the target response, R_o becomes

$$R_o(\rho, \Phi, \Theta) = (2\pi\rho)^2\kappa_o^2\sum_{l=1}^{N_l} r_o^l \left(e(\Phi, \Theta) \cdot [e(\Phi_l, \Theta_l) \otimes \Delta]\right)^2, \tag{16}$$

where κ_o is the user-defined weights for target spatial resolution at the isocenter, and $\{r_o^l\}$ is the pre-defined directional weights, which determines the shape of the target response.

D. Regularization Design

Substituting (15) and (16) into (10) and simplifying yields

$$Q_j(\Phi, \Theta) \approx \frac{\kappa_0^2\tilde{w}_j(\Phi)}{\kappa_j^2\tilde{u}_o(\Phi)}Q_o(\Phi, \Theta), \tag{17}$$

where

$$Q_j(\Phi, \Theta) \triangleq \sum_{l=1}^{N_l} r_j^l \left(e(\Phi, \Theta) \cdot [e(\Phi_l, \Theta_l) \otimes \Delta]\right)^2. \tag{18}$$

We solve the following weighted minimization problem to design the directional weighting coefficient vector $\boldsymbol{r}_j = (r_j^1, \cdots, r_j^{N_l})$ at the jth voxel

$$\begin{aligned} \boldsymbol{r}^j \triangleq \arg\min_{r^j \geq 0} \int_0^{2\pi}\int_{-\frac{\pi}{2}}^{\frac{\pi}{2}} D_w(\Phi, \Theta)|\check{w}_j(\Phi, \Theta)\\ - \sum_{l=1}^{N_l} r_l^j(e(\Phi, \Theta) \cdot [e(\Phi_l, \Theta_l) \otimes \Delta])^2|^2 d\Theta d\Phi, \tag{19} \end{aligned}$$

where the nonnegativity constraint ensures the regularizer's convexity and we define the modified weighting function

$$\check{w}_j(\Phi, \Theta) \triangleq \frac{\kappa_0^2\tilde{w}_j(\Phi)}{\kappa_j^2\tilde{u}_o(\Phi)}\sum_{l=1}^{N_l} r_o^l(e(\Phi, \Theta) \cdot [e(\Phi_l, \Theta_l) \otimes \Delta])^2. \tag{20}$$

We choose $D_w = \cos(\Theta)$ to have more uniform distribution of sampled points. We view (19) as a weighted projection of

$\check{w}_j(\Phi)$ onto the space spanned by $\{[e(\Phi_l, \Theta_l) \otimes \Delta]^2\}$. Inserting the weight $\cos(\Theta)$ into the data-fitting part and expanding this term into 6 orthonormal basis functions, we can decompose $\sum_{l=1}^{N_l} r_j^l \cos^2(\Theta)(e(\Phi, \Theta) \cdot [e(\Phi_l, \Theta_l) \otimes \Delta])^2$ as $\boldsymbol{P}\boldsymbol{T}\boldsymbol{r}^j$, where $\boldsymbol{P}$ is an operator whose columns are the six orthonormal vectors, and $\boldsymbol{T}$ is a $6 \times N_l$ linear combination matrix whose mth row is the following inner product

$$\boldsymbol{T}_{ml} = \frac{1}{2\pi^2} \int_0^{2\pi} \int_{-\pi/2}^{\pi/2} (e(\Phi, \Theta) \cdot [e(\Phi_l, \Theta_l) \otimes \Delta])^2 p_m d\Theta d\Phi. \tag{21}$$

The orthonormal basis functions are given as follows

$$p_1(\Phi, \Theta) = \sqrt{\frac{8}{3}}\cos^2(\Theta)$$

$$p_2(\Phi, \Theta) = \frac{16}{\sqrt{5}}\sin(\Phi)\sin(\Theta)\cos^3(\Theta)$$

$$p_3(\Phi, \Theta) = \frac{16}{\sqrt{5}}\cos(\Phi)\sin(\Theta)\cos^3(\Theta)$$

$$p_4(\Phi, \Theta) = \sqrt{\frac{96}{5}}\cos^2(\Theta)(\cos(2\Theta) - \frac{2}{3})$$

$$p_5(\Phi, \Theta) = \frac{8}{\sqrt{35}}\cos(2\Phi)(1 + \cos(2\Theta))\cos^2(\Theta)$$

$$p_6(\Phi, \Theta) = \frac{32}{\sqrt{35}}\cos^4(\Theta)\cos(\Phi)\sin(\Phi),$$

and assuming $\Delta_x = \Delta_y$, the lth column of $\boldsymbol{T}$ is given by

$$\begin{bmatrix} \sqrt{\frac{3}{2}}(\frac{1}{4}\Delta_x^2\cos^2(\Theta_l) + \frac{1}{3}\Delta_z^2\sin^2(\Theta_l)) \\ \frac{\sqrt{5}}{5}\Delta_x\Delta_z\sin(\Phi_l)\sin(\Theta_l)\cos(\Theta_l) \\ \frac{\sqrt{5}}{5}\Delta_x\Delta_z\cos(\Phi_l)\sin(\Theta_l)\cos(\Theta_l) \\ -\frac{1}{\sqrt{30}}\Delta_z^2\sin^2(\Theta_l) \\ \frac{\sqrt{35}}{28}\Delta_x^2\cos^2(\Theta_l)(\cos^2(\Phi_l) - \sin^2(\Phi_l)) \\ \frac{\sqrt{35}}{14}\Delta_x^2\cos(\Phi_l)\sin(\Phi_l)\cos^2(\Theta_l) \end{bmatrix}.$$

Since $\boldsymbol{P}$ has orthonormal columns, we can represent the minimization problem (19) as the following simplified expression

$$\boldsymbol{r}^j = \arg\min_{\boldsymbol{r} \geq 0} \left\| \boldsymbol{T}\boldsymbol{r} - \boldsymbol{b}^j \right\|^2, \tag{22}$$

where $\boldsymbol{P}^*$ denotes the adjoint of $\boldsymbol{P}$ and $\boldsymbol{b}^j \triangleq \boldsymbol{P}^*\mathring{w}_j(\cdot)$, i.e., $b_k^j = 1/(2\pi^2) \int \int p_k(\Phi, \Theta)\mathring{w}_j(\Phi, \Theta)d\Phi d\Theta$ for $k = 1, \cdots, 6$, where $\mathring{w}_j(\Phi, \Theta) = \check{w}_j(\Phi, \Theta)\cos^2(\Theta)$. The minimization problem (22) is much smaller than (19). We solve (22) using NNLS algorithm [8].

The minimization problem (22) is under-determined and may have many different solutions $\boldsymbol{r}^j$ that are all global minima. Too many zeros in $\boldsymbol{r}^j$ may degrade the image since there will zeros in the Hessian [4]. To ensure that certain $\boldsymbol{r}^j$ values are greater than some small positive number ϵ_l^j, we modity (22) as follows

$$\boldsymbol{r}^j = \arg\min_{\boldsymbol{r} \geq 0} \left\| \boldsymbol{T}\boldsymbol{r} - (\boldsymbol{b}^j - \boldsymbol{T}\boldsymbol{\epsilon}^j) \right\|^2 \tag{23}$$

$$= \arg\min_{\boldsymbol{r} \geq 0} \left\| \boldsymbol{T}\boldsymbol{r} - \bar{\boldsymbol{b}}^j \right\|^2, \tag{24}$$

where $\bar{\boldsymbol{b}}^j \triangleq \boldsymbol{b}^j - \boldsymbol{T}\boldsymbol{\epsilon}^j$. After minimization, we use the coefficients $\bar{\boldsymbol{r}}^j = \boldsymbol{r}^j + \boldsymbol{\epsilon}^j$ for our new regularizer (See [4] for a possible way to select $\boldsymbol{\epsilon}^j$).

III. RESULTS

We simulated a 3rd-generation axial cone-beam CT system using the separable footprint projector [9]. The simulated system has $N_s = 888$ channels and $N_t = 64$ detector rows spaced by $\Delta_s = 1.0239$ mm and $\Delta_t = 1.09878$ mm, and 984 evenly spaced view angles over a 360 degree scan. The source to detector distance was 949 mm, and the source to rotation center distance was 541 mm. We included a quarter detector offset in the channel direction to reduce aliasing. The XCAT phantom [10] was used, and the image was reconstructed to a $512 \times 512 \times 122$ grid with pixel size $\Delta_x = \Delta_y = 0.9766$ mm and $\Delta_z = 0.625$ mm. Poisson noise was added to the sinogram, and the statistical weighting was chosen as $w_i = \exp(-[\boldsymbol{A}\boldsymbol{x}]_i)$. The regularization parameter β was selected such that the target PSF at the isocenter has a full-width at half-maximum (FWHM) of approximately 1.4 mm in xy and 0.9 mm in z.
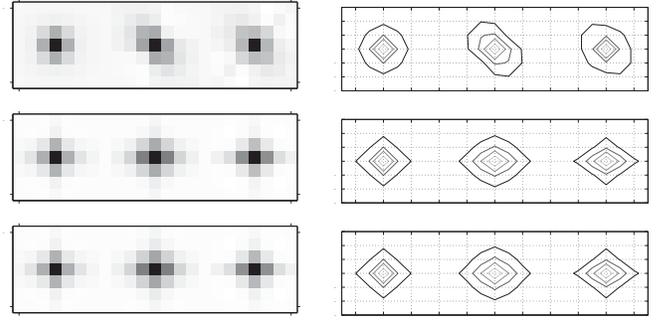
Fig. 1. Impulse responses of conventional regularization (middle column) and proposed regularization (right column) at (-66,217,-17) (mm), which is a fully sampled location. Target impulse response is given as a reference (left column). Each row corresponds to xy, xz, and yz profiles, respectively. Each contour was plotted based on its own peak value.
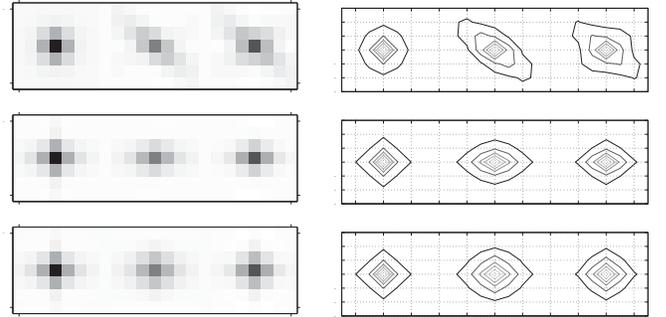
Fig. 2. Impulse responses of conventional regularization (middle column) and proposed regularization (right column) at (-117,-67,17) (mm), which is a insufficiently sampled location. Target impulse response is given as a reference (left column). Each row corresponds to xy, xz, and yz profiles, respectively. Each contour was plotted based on its own peak value.

Figs. 1 and 2 compare impulse responses of conventional regularization and proposed regularization for two different voxels with different sampling properties. There is a considerable anisotropy at both locations, especially for voxels with insufficient sampling. The main reasons for the anisotropy are statistical weighting and scan geometry. The spatial resolution of the voxel in Fig. 1 is primarily affected by the statistical weights, and our proposed method gives more isotropic

impulse response. The location in Fig. 2 is greatly affected by scan geometry, and our proposed method achieves limited improvements.

Fig. 3 compares reconstructed images with various methods. Iteratively reconstructed images show better noise characteristics compared to the FDK reconstruction, but they may have more anisotropic spatial resolution especially at the voxels with less samplings. The true image blurred by the target impulse response was provided as a reference to assess the improvements of our proposed method. In Fig. 4 closely compares the reconstructed images with conventional regularization and the proposed regularization. Overall, the reconstructed image with the proposed regularizer has better resolution characteristics, but has slightly more noise. At locations indicated by the arrows, the proposed regularization shows noticeable improvements (better match to target).
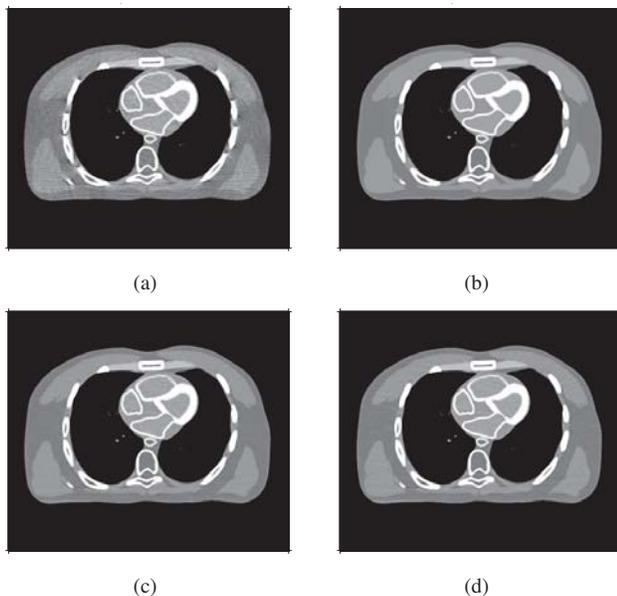
Fig. 3. Reconstructed images at end slice (a) FDK reconstruction (b) True image blurred by the target impulse response (c) Iterative reconstruction with conventional regularizer (d) Iterative reconstruction with designed regularizer

IV. DISCUSSION

We proposed a regularization design method for 3D axial CT that aims to improve resolution uniformity and isotropy. The proposed regularization showed improved spatial resolution characteristics compared to the conventional regularization for the full scan geometry. However, the designed impulse responses do not match the target response precisely and locations with insufficient sampling still suffer from anisotropic resolution. Since 3D axial short scans can suffer from severe anisotropy at the end slices due to their scan geometry, the proposed method may have difficulties achieving desired isotropic resolutions for short scans. We hope to compensate for this with improved regularization design. Furthermore, since edge-preserving regularization is mostly used in practice instead of the quadratic regularization, we will investigate using the designed directional weights in edge-preserving regularization. Our future work will address these issues and focus on refining
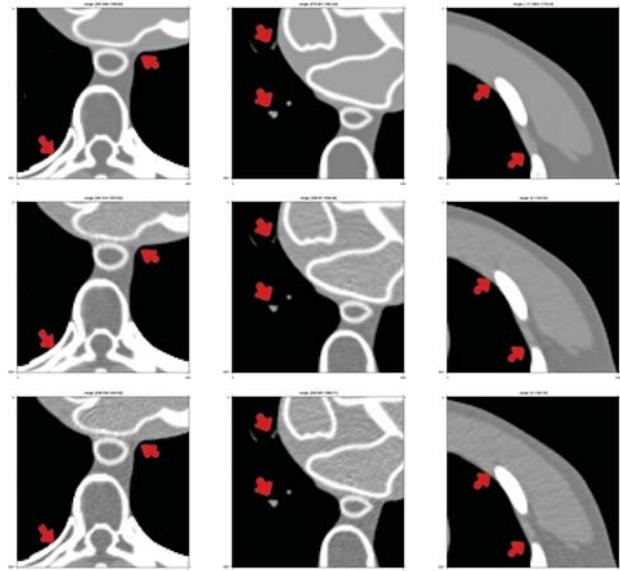
Fig. 4. Reconstructed images with conventional regularization (middle row) and proposed regularization (bottom row) at different locations on end slices. True image blurred by the target impulse response is given as a reference (top row).

the method to obtain better spatial uniformity for different scan geometries and to further improve the computational efficiency of the method.

REFERENCES

[1] J.-B. Thibault, K. Sauer, C. Bouman, and J. Hsieh, "A three-dimensional statistical approach to improved image quality for multi-slice helical CT," *Med. Phys.*, vol. 34, no. 11, pp. 4526–44, Nov. 2007.

[2] J. A. Fessler and W. L. Rogers, "Spatial resolution properties of penalized-likelihood image reconstruction methods: Space-invariant tomographs," *IEEE Trans. Im. Proc.*, vol. 5, no. 9, pp. 1346–58, Sep. 1996.

[3] J. W. Stayman and J. A. Fessler, "Compensation for nonuniform resolution using penalized-likelihood reconstruction in space-variant imaging systems," *IEEE Trans. Med. Imag.*, vol. 23, no. 3, pp. 269–84, Mar. 2004.

[4] H. R. Shi and J. A. Fessler, "Quadratic regularization design for 2D CT," *IEEE Trans. Med. Imag.*, vol. 28, no. 5, pp. 645–56, May 2009.

[5] H. Shi and J. A. Fessler, "Quadratic regularization design for 3D axial CT," in *Proc. IEEE Nuc. Sci. Symp. Med. Im. Conf.*, 2006, pp. 2834–6.

[6] J. Qi and R. M. Leahy, "Resolution and noise properties of MAP reconstruction for fully 3D PET," *IEEE Trans. Med. Imag.*, vol. 19, no. 5, pp. 493–506, May 2000.

[7] S. Schmitt and J. A. Fessler, "Fast variance computation for quadratically penalized iterative reconstruction of 3D axial CT images," in *Proc. IEEE Nuc. Sci. Symp. Med. Im. Conf.*, 2012, pp. 3287–92.

[8] C. L. Lawson and R. J. Hanson, *Solving least squares problems*. Prentice-Hall, 1974.

[9] Y. Long, J. A. Fessler, and J. M. Balter, "3D forward and back-projection for X-ray CT using separable footprints," *IEEE Trans. Med. Imag.*, vol. 29, no. 11, pp. 1839–50, Nov. 2010.

[10] W. P. Segars, M. Mahesh, T. J. Beck, E. C. Frey, and B. M. W. Tsui, "Realistic CT simulation using the 4D XCAT phantom," *Med. Phys.*, vol. 35, no. 8, pp. 3800–8, Aug. 2008.